Analysis on Nanoparticle Growth by Coagulation in Silane Plasma Reactor

Dong-Joo Kim and Kyo-Seon Kim
Dept. of Chemical Engineering, Kangwon National University, Chuncheon, Kangwon-Do, 200-701, Korea

The particle growth in a silane plasma reactor by coagulation between particles was analyzed by using a discrete-sectional model, considering effects of a particle charge distribution based on the Gaussian distribution function. At the start of the plasma discharge, there is the high concentration of small-size particles, and later large-size particles appear and grow by coagulation between small-size particles. Some fractions of small-size particles are in a neutral state or even charged positively. The positively charged small-size particles coagulate faster and more selectively with large-size particles, which are charged more negatively than with medium-size particles. Also, the particle-size distribution in a plasma reactor becomes bimodal and large-size particles become quite monodisperse. As the mass generation rate of monomers increase or as the monomer diameter decreases, large-size particles grow more quickly and the particle-size distribution becomes bimodal earlier. The plasma reactor can be a good candidate to produce monodisperse, nanosized particles.

Introduction

The plasma discharge processes are widely used for semiconductor device manufacturing. These discharges are typically operated at low pressures (tens to hundreds of mTorr) with electron densities of $10^9 - 10^{11}$ cm^{-3}. The plasma processes are quite notorious from the point of particle contamination, and those particles can induce several serious effects on the performance and quality of microelectronic devices and also on the cost of final products. The particles, which vary in size from a few nanometers to microns, are usually found inside the plasma reactor. Some contaminating particles originate outside the plasma process, and other particles can be formed inside the plasma. There are two sources of particles formed inside the plasma: one is a homogeneous formation in the gas phase due to the plasma chemistry, and the other is a heterogeneous formation due to the fracture of deposited thin films. It is believed that those particles grow by coagulation and condensation (Bouchoule and Boufendi, 1994; Boufendi and Bouchoule, 1994; Childs and Gallagher, 2000; Howling et al., 1993; Huang and Kushner, 1997; Kortshagen and Bhandarkar, 1999; Selwyn, 1993, 1994; Shiratani et al., 1996; Watanabe, 1997).

Correspondence concerning this article should be addressed to K.-S. Kim.

Particle contamination control is quite important in the plasma reactor and much research on particle growth has been done theoretically and experimentally. Wantanabe's group (Shiratani et al., 1994, 1996; Watanabe, 1997; Watanabe et al., 1996) analyzed the particle growth in a plasma reactor by the laser light scattering (LLS) methods and proposed that some particles can be charged positively in the plasma reactor. Also, the particles follow three phases (initial growth phase, rapid growth phase, and growth saturation phase) to grow up to submicron sizes. They (Fukuzawa et al., 1999) also studied the particle growth processes in a cluster-size range below a few nm in SiH_4 rf discharges and proposed that the SiH_2 deposition on the particles is important in the initial growth phase, while the particle coagulation becomes important when their density reaches about 10^{11} cm^{-3}. Bouchoule's group (Bouchoule and Boufendi, 1994; Boufendi and Bouchoule, 1994; Bouchoule et al., 1996) suggested the particle growth kinetics for particle sizes from 2 nm to a few 100 nm in an rf-argon-silane plasma and reported that the particles grow rapidly by the coagulation in the first phase and slowly by the surface deposition process on independent particles in the second phase. Hollenstein's group (Howling et al., 1993; Courteille et al., 1996) measured the particle sizes

and concentrations in silane and Ar plasmas by the LLS methods and also modeled the agglomeration phase by the Brownian free molecular coagulation model. Samsonov and Goree (1999) observed that submicron to micron sized particles are produced in the gas phase of sputtering discharges and the growth rate and particle shape vary widely, depending on the target materials. Childs and Gallagher (2000) studied the particle growth in pure silane rf discharge, using an LLS method and showed that the particle density is a sensitive function of gas pressure and rf voltage. Girshick (1997) proposed the particle nucleation by a sequence of reversible chemical reactions and derived the steady-state nucleation rate from the homogeneous nucleation theory.

Most of the particles in plasmas are charged negatively to balance the currents onto the particles by slowly moving ions and fast moving electrons, and particle charging significantly affects the particle growth by coagulation in the plasma reactor. Horanyi and Goertz (1990) considered theoretically the particle growth by enhanced coagulation between the oppositely charged, differently sized grains in the plasma region and suggested that, if the ionization fraction is $\ll 10^{-13}$, the enhanced coagulation might be the most important process responsible for grain growth in the size range of 0.1–500 μm. Lemons et al. (1996) suggested the model equations of particle growth by coagulation of the small neutral particles with the negatively charged large particles to compare with the experimental results by Shiratani et al. (1996) and Boufendi and Bouchoule (1994). Kortshagen and Bhandarkar (1999) studied the growth of nanometer particles in low pressure plasmas and showed that particle coagulation is enhanced compared to coagulation in neutral aerosols due to the attraction of oppositely charged particles. Kim and Ikewawa (1996) and Kim and Kim (1997, 2000a) analyzed the particle formation, growth, and transport in silane plasma reactor with the plasma chemical reactions, which are important for the particle formation in silane plasma reactor and predicted the distributions of those particles inside the plasma reactor for several process conditions based on the neutral particles. Recently, they (Kim and Kim, 2000b) analyzed the rapid particle growth by coagulation between the protoparticles (small sized particles) and the predator particles (large sized particles) in the silane plasma reactor, while considering the Gaussian distribution function for particle charges and showed that most of the large predator particles in the plasma reactor are found to be charged negatively. However, some fractions of small, tiny protoparticles are in a neutral state or even charged positively.

In a previous work (Kim and Kim, 2000b), the particles in the plasma reactor are assumed to have two monodisperse sizes of predator particles and protoparticles, however, in this study, we modified the particle growth model in the silane plasma reactor by considering the particle-size distribution. Also, we could calculate the change of particle-size distribution by applying the discrete-sectional method. We also included the particle charge distribution for each particle size, based on the Gaussian distribution function. The effects of particle charge distribution on coagulation were considered to calculate the particle growth by coagulation in the plasma reactor. The changes of particle-size distribution and particle charge distribution were calculated in the plasma reactor for various process conditions (mass generation rate of monomers, monomer diameter, and initial electron concentration). The predicted model results were also compared with the published experimental data for the same plasma conditions.

Theory

Figure 1 shows the model in this study to predict the particle growth in the plasma reactor. In the plasma reactor dilute with particles, most of those particles will be located around the sheath boundaries and grow there, however, in the plasma reactor dense with particles, the particles are dispersed in the bulk plasma region and are believed to grow by coagulation between particles. Those particles are found to be divided into two groups, small sized and large sized particles (Boufendi and Bouchoule, 1994; Shiratani et al., 1994, 1996; Kim and Kim, 2000b). Our model is to calculate the particle growth by coagulation between particles in the plasma reactor dense with particles. We included the effects of fluid flow, particle generation, particle coagulation, and particle charge distribution on particle growth in plasma reactor.

Most of those particles in the plasma reactor are charged negatively, but, based on the analysis by Matsoukas and Russell (1995), and Matsoukas et al. (1996), some particles in the plasma reactor can be in a neutral state or can be even charged positively, depending on the plasma conditions. They solved the population balance on the stepwise process of particle charging in the plasma reactor and suggested that the charge distribution of particles above a few nms can be expressed as the Gaussian distribution function. The particle charge distribution ($f(z)$), average charge ($\bar{z}_l$) and variance (σ_l^2) of the distribution were expressed by Eqs. 1–3, respectively, in terms of particle diameter (d_l), concentrations of electron and positive ion (N_e, N_+), masses of electron and positive ion (M_e, M_+) and temperatures of electron and positive ion (T_e, T_+) (Matsoukas and Russell, 1995; Matsoukas et al., 1996; Kim and Kim, 2000b)

$$f(z) = \frac{1}{\sigma_l \sqrt{2\pi}} \exp\left[-\frac{(z - \bar{z}_l)^2}{2\sigma_l^2} \right] \tag{1}$$

$$\bar{z}_l \approx C \frac{2\pi \epsilon_0 d_l k_B T_g}{e^2} \ln \frac{N_+}{N_e} \left(\frac{M_e T_e}{M_+ T_+} \right) \tag{2}$$

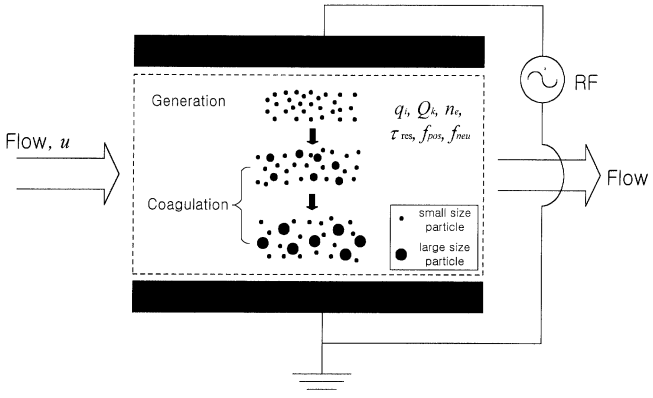

Figure 1. Model of particle growth in silane plasma reactor.

$$\sigma_l^2 = \left(\frac{1}{\beta_e}\right)\left(\frac{1 - t'\beta_e \bar{z}_l}{t' + 1 - t'\beta_e \bar{z}_l}\right) \tag{3}$$

where β_e and t' are defined as

$$\beta_e = \frac{e^2}{2\pi\epsilon_0 d_l k_B T_g}; \qquad t' = \frac{T_e}{T_+} \tag{4}$$

We assumed the bulk plasma region in the plasma reactor is the continuously stirred-tank reactor and the gas stream has the residence time of τ_{res} inside the plasma reactor. The general dynamic equation for particles in plasma reactor is given as follows

$$\frac{dn(v)}{dt} = I(v)\delta(v - v_1) + \frac{1}{2}\int_{v_1}^{v} E(\bar{v}, v - \bar{v})\beta(\bar{v}, v - \bar{v})n(\bar{v})n(v - \bar{v})d\bar{v} - \int_{v_1}^{\infty} E(v, \bar{v})\beta(v, \bar{v})n(v)n(\bar{v})d\bar{v} - (F_{\text{pos}} + F_{\text{neu}})\frac{n(v)}{\tau_{\text{res}}} \tag{5}$$

The first term on the righthand side of Eq. 5 shows the monomer generation rate and the second and the third terms, the particle generation, and disappearance rates by particle coagulation, respectively. The $E(v, \bar{v})$ is the enhancement factor of the collision frequency function taking into account the particle charge distribution of colliding particles. The last term on the righthand side of Eq. 5 shows the disappearance rate by fluid flow. It is assumed that the particles which are charged positively or in a neutral state go out of the reactor with fluid flow, but the particles charged negatively are caught inside the plasma reactor by the electrostatic repulsion in the sheath region.

Equation 5 is a nonlinear, partial integro-differential equation and an appropriate approach should be used to solve this equation to predict the evolution of the particle-size distribution within limited computing time. The discrete-sectional model (Gelbard et al., 1980; Wu and Flagan, 1988) can reduce the computing time, but predict the evolution of particle-size distribution quite well. We applied the discrete-sectional model modified by Landgrebe and Pratsinis (1990) and Wu and Biswas (1998) to analyze the particle growth by coagulation between charged particles in plasma reactor. The aerosol size spectrum for discrete-sectional model is well illustrated by Gelbard et al. (1980), Wu and Flagan (1988), and Kobata et al. (1991), and the q_i is the volume concentration of particles containing i monomers in discrete-size regime (DSR). The Q_k is the volume concentration of particles in size between v_{k-l} and v_k in sectional-size regime (SSR) and is defined as follows

$$Q_k = \int_{v_{k-1}}^{v_k} n(v)v\,dv \tag{6}$$

The volume-conserved discrete-sectional model we applied is good at predicting the particle-size distribution where particles grow by coagulation (Wu and Biswas, 1988). The population balance for the monomers from the general dynamic equation can be expressed as

$$\frac{dq_1}{dt} = \frac{S_1}{\rho_d} - q_1 \sum_{j=1}^{i\max} \left(E_{1,j}\beta^*_{1,j}q_j\right) - q_1 \sum_{k=1}^{k\max} \left(E_{1,k}{}^4\bar{\beta}^D_{1,k}Q_k\right) - \left(F_{\text{pos},1} + F_{\text{neu},1}\right)\frac{q_1}{\tau_{\text{res}}} \tag{7}$$

The first righthand side term of Eq. 7 is the generation rate of monomers, and the second and third terms are the disappearance rates of monomers by coagulation with particles in DSR and SSR, respectively. The last righthand side term is the loss rate of q_1 by fluid flow. The population balance for i-mers ($i = 2$ to $i\max$) is

$$\frac{dq_i}{dt} = \frac{1}{2}\sum_{j=1}^{i-1} \left(E_{j,(i-j)}\beta^*_{j,(i-j)}q_j q_{(i-j)}\right) - q_i \sum_{j=1}^{i\max} \left(E_{i,j}\beta^*_{i,j}q_j\right) - q_i \sum_{k=1}^{k\max} \left(E_{i,k}{}^4\bar{\beta}^D_{i,k}Q_k\right) - \left(F_{\text{pos},i} + F_{\text{neu},i}\right)\frac{q_i}{\tau_{\text{res}}} \tag{8}$$

The first righthand side term of Eq. 8 is the generation rate of q_i by coagulation of smaller particles and the next two terms are the disappearance rates of q_i by coagulation of i-mers with DSR and SSR particles, respectively.

The population balance for the first section is

$$\frac{dQ_1}{dt} = \frac{1}{2}\sum_{i=1}^{i\max}\sum_{j=1}^{i\max} \left(E_{i,j}{}^1\bar{\beta}^{DD}_{i,j,1}q_i q_j\right) - Q_1 \sum_{i=1}^{i\max} \left(E_{i,1}{}^2\bar{\beta}^D_{i,1}q_i\right) + Q_1 \sum_{i=1}^{i\max} \left(E_{i,1}{}^5\bar{\beta}^D_{i,1}q_i\right) - \frac{1}{2}E_{1,1}{}^3\bar{\beta}_1 Q_1^2 - Q_1 \sum_{i=2}^{k\max} \left(E_{i,1}{}^4\bar{\beta}_{i,1}Q_i\right) - \left(F_{\text{pos},(i\max+1)} + F_{\text{neu},(i\max+1)}\right)\frac{Q_1}{\tau_{\text{res}}} \tag{9}$$

The first righthand side term is the generation rate of Q_1 by coagulation between two DSR particles. The second and third righthand side terms are the loss and generation rates, respectively, of Q_1 from coagulations between particles in DSR and in the first section. The fourth and fifth righthand side terms are the loss rates of Q_1 by coagulations between two first section particles and between first section and larger section particles, respectively. The final righthand side term is the effect of fluid flow. The population balance equation for the kth section ($k = 2$ to $k\max$) is

$$\frac{dQ_k}{dt} = \frac{1}{2}\sum_{i=1}^{i\max}\sum_{j=1}^{i\max} \left(E_{i,j}{}^1\bar{\beta}^{DD}_{i,j,k}q_i q_j\right) + \sum_{i=1}^{i\max}\sum_{j=1}^{k-1} \left(E_{i,j}{}^1\bar{\beta}^D_{i,j,k}q_i Q_j\right) + \frac{1}{2}\sum_{i=1}^{k-1}\sum_{j=1}^{k-1} \left(E_{i,j}{}^1\bar{\beta}_{i,j,k}Q_i Q_j\right) - Q_k \sum_{i=1}^{i\max} \left(E_{i,k}{}^2\bar{\beta}^D_{i,k}q_i\right)$$

$$+ Q_k \sum_{i=1}^{i\max} \left({E_{i,k}}^5 \overline{\beta}_{i,k}^D q_i \right) - Q_k \sum_{i=1}^{k-1} \left({E_{i,k}}^2 \overline{\beta}_{i,k} Q_i \right)$$

$$+ Q_k \sum_{i=1}^{k-1} \left({E_{i,k}}^5 \overline{\beta}_{i,k} Q_i \right) - \frac{1}{2} {E_{k,k}}^3 \overline{\beta}_k Q_k^2 - Q_k \sum_{i=k+1}^{k\max}$$

$$\times \left({E_{i,k}}^4 \overline{\beta}_{i,k} Q_i \right) - \left(F_{\mathrm{pos},(i\max+k)} + F_{\mathrm{neu},(i\max+k)} \right) \frac{Q_k}{\tau_{\mathrm{res}}} \quad (10)$$

The first three righthand side terms are the generation rates of Q_k by coagulations between two DSR particles, between one DSR and one smaller SSR particle, and between two smaller SSR particles, respectively. The fourth and fifth righthand side terms are the disappearance and generation rates, respectively, of Q_k by coagulations between one DSR and one section-k particle. The sixth and seventh righthand side terms are the disappearance and generation rates, respectively, of Q_k by coagulations between one smaller SSR and one section-k particle. The eighth and ninth righthand side terms, respectively, are the loss rates of Q_k by coagulations between two section-k particles and between one section-k and one larger section particle. The final righthand side term accounts for the loss of Q_k by fluid flow.

All the particles in plasma reactor will be charged or in neutral state and the fractions of particles in DSR and SSR, which are charged negatively or positively or in a neutral state, can be calculated from the Gaussian distribution function of particle charging. The fractions of particles which are charged negatively, neutral, or charged positively ($F_{l,\mathrm{neg}}$, $F_{l,\mathrm{neu}}$, $F_{l,\mathrm{pos}}$) in DSR and SSR and also the average charges of the negatively and positively charged particles ($\bar{z}_{l,\mathrm{neg}}$, $\bar{z}_{l,\mathrm{pos}}$) in DSR and SSR can be calculated from the Gaussian distribution function of particle charges in terms of particle size and plasma parameters (Kim and Kim, 2000b).

$$F_{l,\mathrm{neg}} = \int_{-\infty}^{-0.5} f(z)dz = \frac{1}{2} - \frac{1}{2} \mathrm{erf}\left(\frac{-x_{l,1}}{\sqrt{2}} \right) \quad (11)$$

$$F_{l,\mathrm{neu}} = \int_{-0.5}^{0.5} f(z)dz = \frac{1}{2}\left[\mathrm{erf}\left(\frac{-x_{l,1}}{\sqrt{2}} \right) + \mathrm{erf}\left(\frac{x_{l,2}}{\sqrt{2}} \right) \right] \quad (12)$$

$$F_{l,\mathrm{pos}} = \int_{0.5}^{\infty} f(z)dz = \frac{1}{2} - \frac{1}{2}\left[\mathrm{erf}\left(\frac{x_{l,2}}{\sqrt{2}} \right) \right] \quad (13)$$

$$\bar{z}_{l,\mathrm{neg}} = \frac{\int_{-\infty}^{-0.5} f(z) z dz}{\int_{-\infty}^{-0.5} f(z)dz} = -\frac{\sigma_l \ \mathrm{Exp}\left[-\frac{x_{l,1}^2}{2} \right]}{\int_{-\infty}^{x_{l,1}} f(z)dz} + \bar{z}_l \quad (14)$$

$$\bar{z}_{l,\mathrm{pos}} = \frac{\int_{0.5}^{\infty} f(z) z dz}{\int_{0.5}^{\infty} f(z)dz} = \frac{\sigma_l \ \mathrm{Exp}\left[-\frac{x_{l,2}^2}{2} \right]}{\int_{x_{l,2}}^{\infty} f(z)dz} + \bar{z}_l \quad (15)$$

In Eqs. 11–15, $x_{l,1}$ and $x_{l,2}$ are defined as $(-0.5-\bar{z}_l)/\sigma_l$ and $(0.5-\bar{z}_l)/\sigma_l$, respectively. The average electron charge on particles is proportional to particle diameter, and the large sized particles will be charged more negatively than the small sized particles. The smaller particles ($d \le 10$'s nm) can have more possibility of being neutral or even being charged positively, depending on the plasma conditions (Kim and Kim, 2000b). The particles of opposite charges will collide with each other very fast and the neutral particles can collide with all particles, but the particles of same charges cannot collide together. We assumed that the particle charge in plasmas is concentrated and fixed at the center of the particle, and we neglected the effect of image forces on particle coagulation, resulting from the charge separation in solid particles (Xiong et al., 1992; Matsoukas and Russell, 1997). The $E_{i,j}$ in Eqs. 7–10 can be calculated as follows

$$E_{i,j} = \left[F_{i,\mathrm{neu}} F_{j,\mathrm{neu}} + F_{i,\mathrm{neu}} F_{j,\mathrm{neg}} + F_{i\mathrm{neu}} F_{j,\mathrm{pos}} \right.$$
$$+ F_{i,\mathrm{neg}} F_{j,\mathrm{neu}} + F_{i,\mathrm{neg}} F_{j,\mathrm{pos}} \left(1-\Gamma_{i,j}\right) + F_{i,\mathrm{pos}} F_{j,\mathrm{neu}}$$
$$\left. + F_{i,\mathrm{pos}} F_{j,\mathrm{neg}} \left(1-\Gamma_{i,j}\right) \right] \quad (16)$$

$$\Gamma_{i,j} = \frac{\bar{z}_{i,(\mathrm{neg\ or\ pos})} \bar{z}_{j,(\mathrm{pos\ or\ neg})} e^2}{\pi \epsilon_0 m_R v_R^2 \left(d_i + d_j \right)} \quad (17)$$

$(1-\Gamma_{i,j})$ in Eq. 16 is the enhancement factor of collision frequency function induced by the Coulomb force between the oppositely charged particles colliding together. If the positive and negative charges per unit volume do not compensate, the particle loss due to electrostatic dispersion can occur and the particle-size distribution can be affected (Kasper, 1981; Adachi et al., 1981; Vemury et al., 1997). As we solve the electroneutrality condition in the plasma reactor, we can neglect the effect of charged particle dispersion losses.

The electrons are absorbed onto the particles and the electron concentration changes with time as the particle concentration and size change in the plasma reactor. We included the electroneutrality condition in the plasma reactor by considering the charges by electrons, positive ions, negative ions and particles as follows

$$N_e = N_+ - N_- + \sum_{l=1}^{i\max + k\max} N_l \bar{z}_l \quad (18)$$

By inserting $\bar{z}_l$ in Eq. 2 into Eq. 18, we have Eq. 19

$$N_e = B_1 - B_2 \ln N_e \quad (19)$$

The B_1 and B_2 are defined as

$$B_1 = N_+ - N_- + \sum_{l=1}^{i\max + k\max} N_l A_{1,l}$$

$$B_2 = \sum_{l=1}^{i\max + k\max} N_l A_{2,l}$$

where

$$A_{1,l} = C \frac{2\pi\epsilon_0 d_l k_B T_e}{e^2} \ln N_+ \left(\frac{M_e T_e}{M_+ T_+} \right)^{1/2}$$

$$A_{2,l} = C \frac{2\pi\epsilon_0 d_l k_B T_e}{e^2}$$

We assumed that the positive and negative ion concentrations in the plasma reactor are constant and solved the Eq. 19 by the Newton-Raphson method (Riggs, 1988) to calculate the change of electron concentration with time. The electroneutrality condition (Eq. 19) will not be satisfied in the sheath region of plasma reactor, but will be satisfied in the bulk plasma and approximately in the sheath boundary region.

In this computation, the number of discrete sizes ($i$max) is 20, which are quite enough to avoid the inaccuracies at the junction of the discrete and sectional parts (Wu and Flagan, 1988). The section spacing (v_k/v_{k-1}) in SSR was 1.05. Equations 7–10 were solved numerically by the ODE solver, the DGEAR subroutine, to calculate the particle-size distribution in the plasma reactor by the discrete-sectional model. In every time step of integration, the electroneutrality condition (Eq. 19) was also solved to calculate the electron concentration. The particle charge distributions, the fractions of negatively charged, neutral, or positively charged particles, and the average charges of particles were also calculated from the electron concentration. The $E_{i,j}$ were calculated in every time step of integration by Eqs. 16 and 17 and were implemented into the population balance equations in DSR and SSR to calculate the coagulation rates between particles.

Results and Discussions

The changes of particle-size distribution and particle charge distribution were calculated in a plasma reactor, changing several process conditions such as mass generation rate of monomers (S_1), monomer diameter (d_1), and initial electron concentration ($N_{e,0} = N_+ - N_-$). The standard conditions for S_1, d_1 and τ_{res} were 4.23×10^{-7} g/cm^3·s, 10 nm and 0.485 s (30 std cm^3), respectively, which were the experimental conditions by Shiratani et al. (1996). The positive and negative ion concentrations in the plasma reactor reach the steady state very quickly in comparison to the particle growth time, and we assumed that those concentrations are constant. The concentrations of positive ions (N_+) and negative ions (N_-) were found by the numerical program (Kim and Kim, 1997) in silane PCVD for the conditions of pressure = 0.6 Torr, gas temperature = 300 K, and total gas-flow rate = 30 std cm^3 and were about 6.0×10^{10} cm^{-3} and 5.0×10^{9} cm^{-3}, respectively. The positive ion concentration is usually measured to be less than 10^{10} cm^{-3}, but at a high frequency of discharge, can be higher than 10^{10} cm^{-3} (Shiratani et al., 1994; Watanabe et al., 1996). The standard condition for $N_{e,0}$ becomes 5.5×10^{10} cm^{-3}. The plasma conditions for ion temperature (T_+) and electron temperature (T_e) were assumed to be 300 K and 2 eV, respectively.

Figures 2 and 3 show the changes of particle-size distribution for various times and the changes of particle charge distributions for various particle sizes in the plasma reactor, respectively. Just after the plasma discharge on ($t \cong 0.05$ s), we have only the small-size particles, which start to grow by coagulation between particles, and, later, the large-size particles appear ($t \cong 0.3$ s) and grow larger and larger. Finally, the large-size particles are separated from the small sized particles (Figure 2). As the particle size increases, the surface area of particles for collision with electrons increases, and, in Fig-

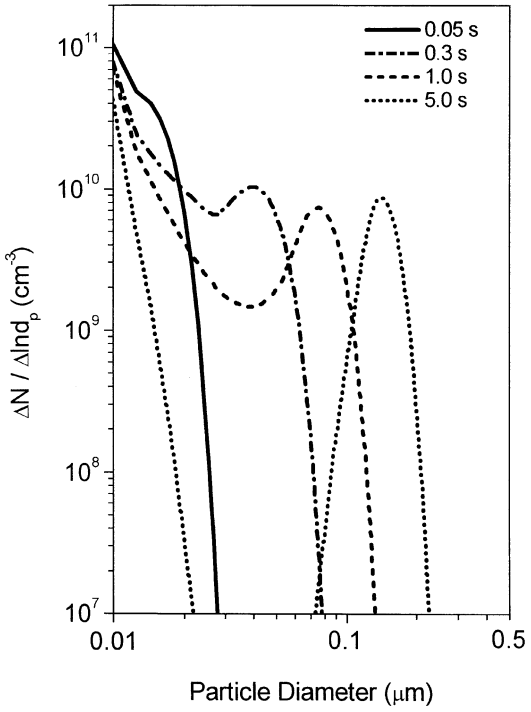

Figure 2. Particle-size distributions in plasma reactor for various times.

$S_1 = 4.23\times10^{-7}$ g/cm^3·s, $d_1 = 10$ nm, $\tau_{res} = 0.485$ s, $N_{e,0} = 5.5\times10^{10}$ cm^{-3}.

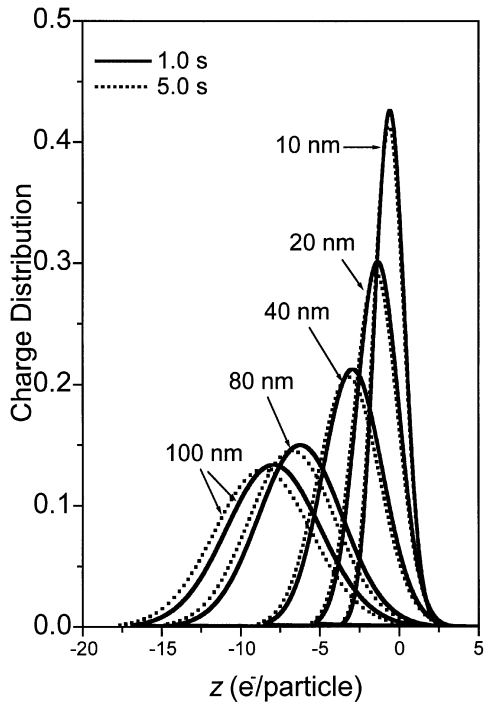

Figure 3. Particle charge distributions in plasma reactor for various particle sizes.

$S_1 = 4.23\times10^{-7}$ g/cm^3·s, $d_1 = 10$ nm, $\tau_{res} = 0.485$ s, $N_{e,0} = 5.5\times10^{10}$ cm^{-3}.

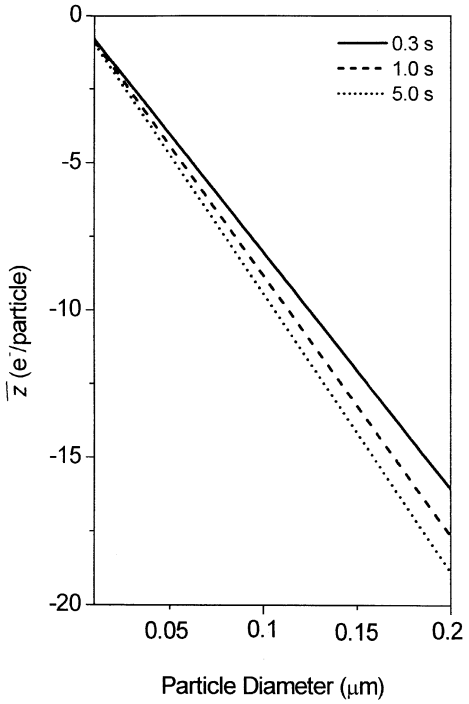

Figure 4. Average number of electrons per particle for various times.

$S_1 = 4.23 \times 10^{-7}$ g/cm^3·s, $d_1 = 10$ nm, $\tau_{res} = 0.485$ s, $N_{e,0} = 5.5 \times 10^{10}$ cm^{-3}.

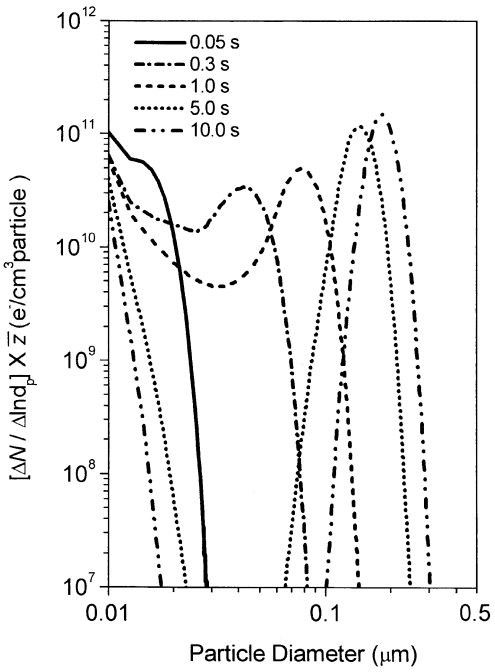

Figure 5. Amount of particle charges absorbed onto each particle size for various times.

$S_1 = 4.23 \times 10^{-7}$ g/cm^3·s, $d_1 = 10$ nm, $\tau_{res} = 0.485$ s, $N_{e,0} = 5.5 \times 10^{10}$ cm^{-3}.

ure 3, the large-size particles are charged more negatively than the small-size particles. Most of large-size particles ($d =$ 100 nm) are charged negatively, but, for the case of small-size particles ($d = 10$ nm), we can see that some fractions of small-size particles are in a neutral state and some fractions are, surprisingly, charged positively (Figure 3). The small-size particles charged positively can coagulate very fast with the large-size particles charged negatively by the electrostatic attraction. The small-size particles will coagulate more rapidly with the large-size particles, which are charged more negatively than with the medium-size particles, and the large-size particles grow faster than the medium-size particles. The disappearance rate of particles in the kth section by the coagulation with small-size particles is greater than the generation rate of particles by the coagulation between small-size particles and one smaller section of particles, because the particles in the kth section are charged more negatively than the particles in the smaller section. As a result, the medium-size particles are depleted and we can see a clear discrepancy in the particle-size distribution between large-size and small-size particles in Figure 2 at $t = 5$ s. Also, the particle-size distribution in the plasma reactor becomes bimodal. As the concentration of the medium-size particles becomes quite low, the large-size particles cannot be generated any more and the concentration of large sized particles becomes almost constant. The integral correction factor (W) for coagulation between charged particles is proposed by Friedlander (2000). The W for 10 nm particles of -1 e^-/particle is 4.11×10^{13} and the coagulation between particles of same charges can be neglected.

Figures 4 and 5 illustrate the average number of electrons per particle and the amount of particle charges absorbed onto each particle size (particle-size distribution $\times$ average charges of the particle size), respectively, for various times. The area under the curve in Figure 5 is the amount of negative charges on particles. As the particle size increases, the average number of electrons per particle increases because the large sized particles are charged more negatively (Figure 4). The average number of electrons per particle at high particle concentration is lower compared to the particles in undisturbed plasma (Matsoukas and Russell, 1997). The Gaussian particle charge distribution is based on the assumption that the bombardment rates between particles and ions and electrons are much faster than the rate of coagulation so that a particle after coagulation attains its equilibrium charge before another coagulation. The charging time of an initially neutral particle increases as the particle size decreases, and it is calculated about 34.5 μs for 10 nm particles, while about the characteristic time of coagulation of 10 nm particles is about 4,000 μs. Also, we could see that new particles are equilibrated in particle charges before another coagulation. At 0.05 s, there are low concentrations of large sized particles (Figure 2) and most of the electrons are absorbed into small sized particles. Later, the large size particles appear and grow (Figure 2), they are charged more negatively, and the amount of particle charges absorbed onto the large sized particles increases (Figure 5). At 5 s, the amount of electrons absorbed onto the large sized particles ($\cong 78\%$) are larger than those on the small sized particles ($\cong 22\%$). We can see that, for 5 s $\le t \le$ 10 s, the amounts of negative charges on large sized particles are almost the same, but the amount of negative charges on small

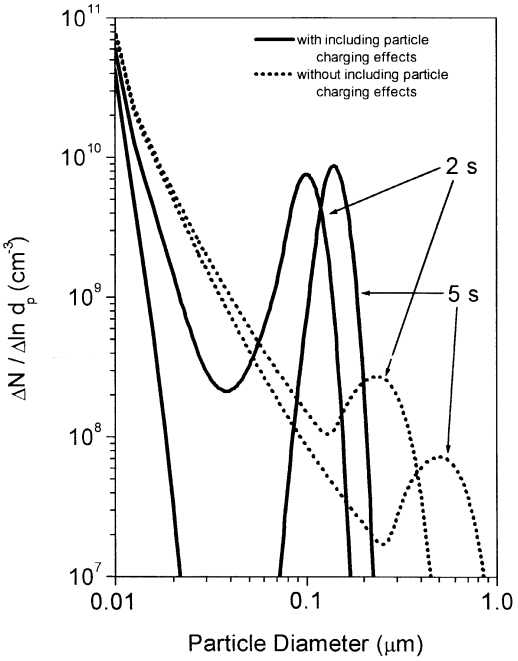

Figure 6. Particle-size distributions: with vs. without including particle charging effects for various times.

$S_1 = 4.23 \times 10^{-7}$ g/cm^3·s, $d_1 = 10$ nm, $\tau_{res} = 0.485$ s, $N_{e,0} = 5.5 \times 10^{10}$ cm^{-3}.

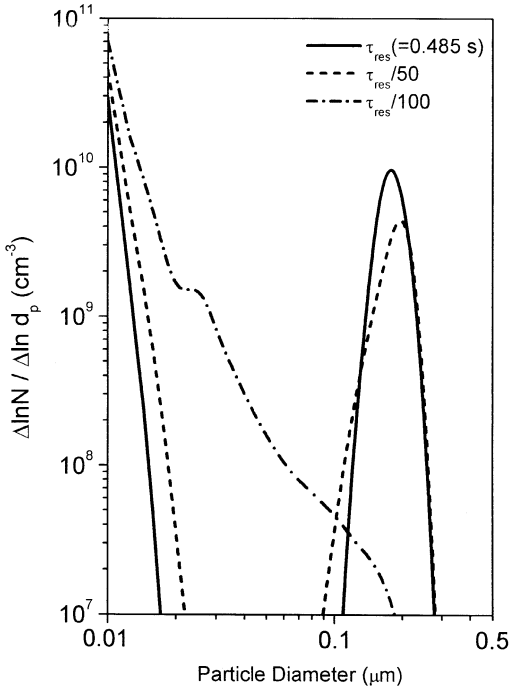

Figure 7. Particle-size distributions in plasma reactor for various residence times at 10 s.

$S_1 = 4.23 \times 10^{-7}$ g/cm^3·s, $d_1 = 10$ nm, $N_{e,0} = 5.5 \times 10^{10}$ cm^{-3}.

sized particles decreases (Figure 5). In addition the total amount of negative charges onto the particles decreases with time. The electron concentration in plasma reactor increases slightly with time (at $t = 0.3$ s, $N_e = 2.6 \times 10^9$ cm^{-3}, at $t = 5$ s, $N_e = 2.67 \times 10^9$ cm^{-3}, at $t = 10$ s, $N_e = 2.7 \times 10^9$ cm^{-3}) and particles of the same size become charged more negatively with time (Figure 4).

The particle charging is a very unique and important phenomena to explain the particle growth in the plasma reactor. In the usual aerosol reactors, the particles grow by coagulation between the neutral particles (without including particle charging). Figure 6 presents the comparison of particle-size distributions with and without including the particle charging effects in the plasma reactor. While including particle charging, the small sized particles charged positively will coagulate more selectively with the large sized particles charged more negatively than with the medium-size particles, and the particle-size distribution becomes bimodal. Additionally, the large sized particles become quite monodisperse. On the other hand, if not including particle charging, all sized particles can coagulate with each other and the medium sized particles can be generated and grow by coagulation between particles and, as a result, the particle-size distribution becomes broader and the large-size particles become bigger than with including particle charging. In this sense, the plasma reactor where the particle charging is quite significant can be a good candidate to produce monodisperse, nanosized particles.

The particles which are charged positively and in a neutral state are lost by the fluid flow, and Figure 7 shows the change of particle-size distribution for various residence times. As the residence time decreases, it takes a longer time for the large-size particles to appear by coagulation with small-size particles, because more of small-size particles which are charged positively or in a neutral state are lost by the fluid

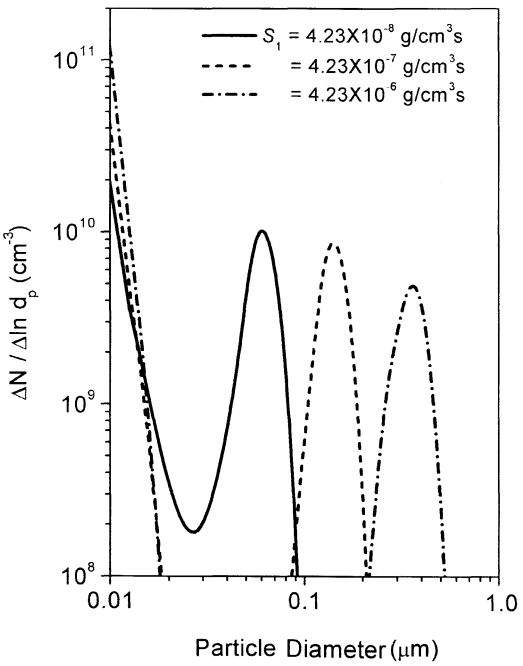

Figure 8. Particle-size distributions in plasma reactor for various mass generation rates of monomers at 5 s.

$d_1 = 10$ nm, $\tau_{res} = 0.485$ s, $N_{e,0} = 5.5 \times 10^{10}$ cm^{-3}.

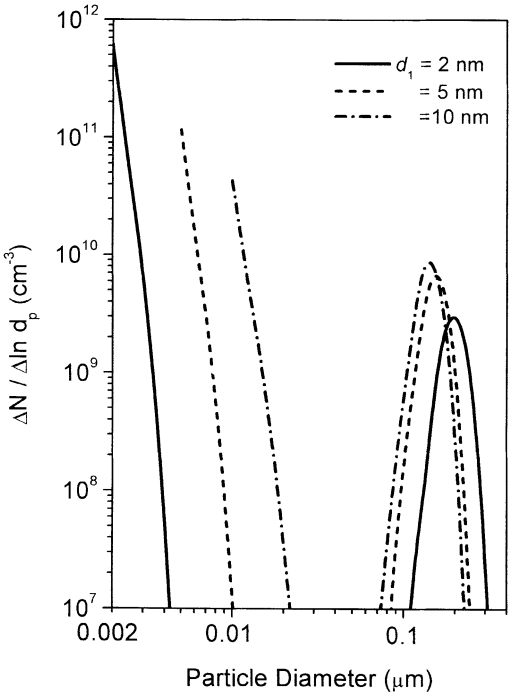

Figure 9. Particle-size distributions in plasma reactor for various monomer diameters at 5 s.

$S_1 = 4.23 \times 10^{-7}$ g/cm^3·s, $\tau_{res} = 0.485$ s, $N_{e,0} = 5.5 \times 10^{10}$ cm^{-3}.

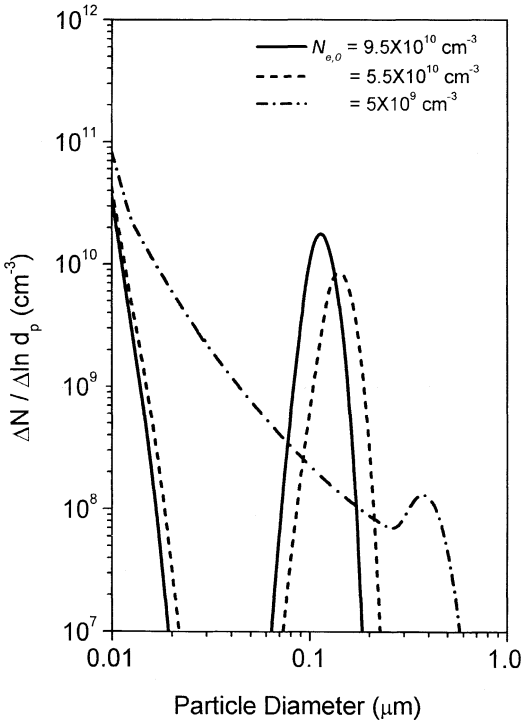

Figure 10. Particle-size distributions in plasma reactor for various initial electron concentrations at 5 s.

$S_1 = 4.23 \times 10^{-7}$ g/cm^3·s, $d_1 = 10$ nm, $\tau_{res} = 0.485$ s.

flow. The large-size particles are mostly charged negatively and the large-size particles are not affected significantly by the fluid flow if they are formed once.

Figures 8 and 9 show the changes of particle-size distributions at 5 s for various mass generation rates of monomers and for various monomer diameters, respectively. The particle-size distributions are again bimodal with small-size and large-size particles. As the monomer generation rate increases, small-size particle concentration increases and the large-size particles grow more quickly and become larger by the faster coagulation with the small sized particles. Additionally, the particle-size distribution becomes bimodal earlier (Figure 8). As the monomer diameter decreases, the small-size particle concentration becomes higher because the number of monomers generated increases for the given mass generation rate of monomers. The large-size particles grow more quickly by the faster coagulation with small-size particles of higher concentration, and the large-size particles are separated more clearly from the small-size particles (Figure 9).

Figure 10 describes the change of the particle-size distribution for various initial electron concentrations ($N_{e,o}$) in the plasma reactor. As the initial electron concentration increases, the fractions of small-size particles charged positively and in a neutral state decrease, and the large-size particles which are charged negatively cannot grow quickly by coagulation with the small-size particles and the large-size particles become smaller. The particle charge distribution with a small initial electron concentration of $N_{e,0} = 5 \times 10^9$ cm^{-3} is shown in Figure 11, and we can see that a significant amount of particles in plasma reactor are in a neutral state.

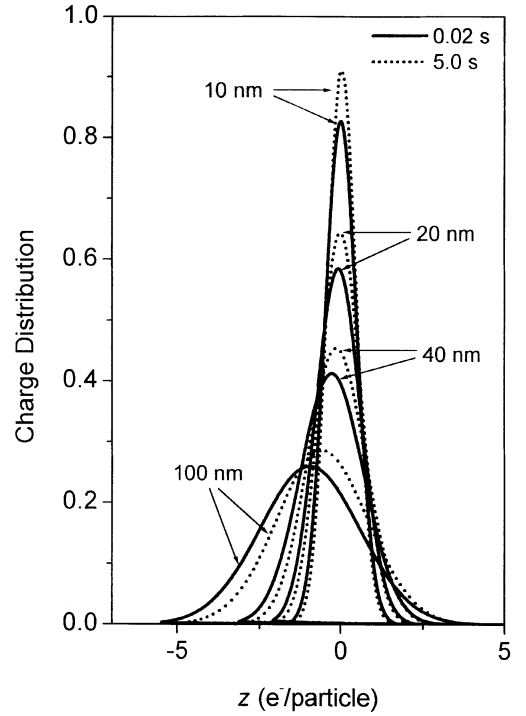

Figure 11. Particle charge distributions in plasma reactor for various times at $N_{e,0} = 5.0 \times 10^9$ cm^{-3}.

$S_1 = 4.23 \times 10^{-7}$ g/cm^3·s, $d_1 = 10$ nm, $\tau_{res} = 0.485$ s.

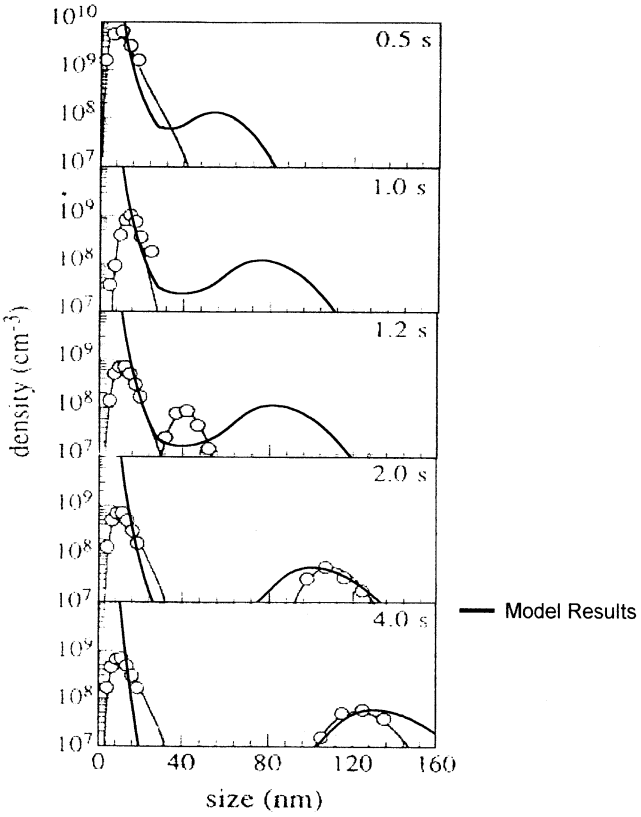

Figure 12. Predicted particle-size distributions vs. experimental results by Shiratani et al. (1996).

Also, in Figure 10, the particle-size distribution becomes broader and the large-size particles become bigger (same as shown in Figure 7 for neutral particles without including particle charging).

Figure 12 shows the comparison of model results in this study with the published experimental data by Shiratani et al. (1996) for the same process conditions ($S_1 = 4.23 \times 10^{-7}$ g/cm^{3}s, $d_1 = 10$ nm, and $\tau_{res} = 0.485$ s). In their experiments, the small-size particles are observed in the beginning of discharge ($t \leq 1$ s) and, later, the large-size particles appear ($t =$ 1.2 s) and are separated from the small-size particles ($t = 2$ s) and grow ($t = 4$ s), as we predicted qualitatively in our model results. Our model results at $t = 2$ s and 4 s are in quite good agreement with their experimental results. Our model results become bimodal earlier than the experimental data, and the predicted small-size particle distribution is not a log-normal as the experimental ones. The reasons for those differences might be explained in this study. In our model, we assumed that the mass generation rate of monomer is constant and the particles grow rapidly by coagulation from the beginning of discharge, but they (Shiratani et al., 1994, 1996; Watanabe, 1997) proposed that the particles follow the first initial growth phase of nucleation for 0 s $\leq t \leq$ 0.5 s and, after that, follow the rapid particle growth phase by coagulation. Also the N_+ concentration in our model is higher than the experimental measurements. If the phenomena of monomer generation and coagulation between particles are important as in this model, the small-size particle distribution cannot be a log-normal type as in their experiments. We also compare our model results of average large-size particle diameter by a discrete-sectional method after the large-size particles appear ($t \geq 1$ s) with those by a two-sized particle growth model (Kim and Kim, 2000b). Just after the large sized particles appear ($t \geq 1$ s), the large-size particles in the two-size particle growth model are bigger than in the discrete-sectional model because the large sized particles in the two-sized particle growth model have grown from the beginning, however, after 5 s, the large-size particles in the discrete-sectional model become bigger than in the two-size particle growth model, because the collision frequency function between different particle sizes is higher than between the same sized particles (Friedlander, 2000).

Conclusions

We analyzed the particle growth in the silane plasma reactor by using a discrete-sectional model and the particle coagulation rate was calculated considering the effects of particle charge distribution based on the Gaussian distribution function. The changes of particle-size distribution and particle charge distribution were calculated in the plasma reactor for various process conditions (mass generation rate of monomers, monomer diameter, and initial electron concentration).

Just after the plasma discharge, we have the high concentration of small-size particles and, later, the large-size particles appear by coagulation between small-size particles and grow bigger and, finally, the large-size particles are separated from the small size particles. Most of the particles in the plasma reactor are charged negatively and, the larger the particles size is, the more negatively the particles are charged. It is found that some fractions of small-size particles are in a neutral state or even charged positively. The small-size particles positively charged will coagulate more rapidly with the large-size particles, which are charged more negatively than with the medium-size particles, and the medium-size particles are depleted and the particle-size distribution becomes bimodal and the large-size particles become quite monodisperse. These results show that the plasma reactor can be used to produce monodisperse, nanosized particles.

As the mass generation rate of monomers increases or as the monomer diameter decreases, the small-size particle concentration increases and the large-size particles grow more quickly by the faster coagulation with the small-size particles, and the particle-size distribution becomes bimodal earlier. As the initial electron concentration increases, the small-size particle concentration charged positively decreases and the large-size particles, which are charged negatively, cannot grow fast by coagulation with the small sized particles charged positively. With small initial electron concentration ($N_{e,0} = 5 \times 10^9$ cm^{-3}), a significant amount of particles in the plasma reactor are in a neutral state and the particle-size distribution becomes broader and the large sized particles grow more quickly.

The model results of particle-size distributions in this study were in good agreement with the published experimental data (Shiratani et al., 1996). We believe this analysis can be applied to understand the nanosized particle growth in a plasma reactor.

Acknowledgments

This work was supported by Korea Research Foundation Grant (KRF-2000-015-DP0117) and also by grant No. R01-2000-00329 from Korea Science and Engineering Foundation.

Notation

C = constant, 0.73
d_l = particle diameter in the lth discrete size regime or sectional size regime, cm
d_1 = monomer diameter, cm
e = elementary charge of electron, C
$f(z)$ = particle charge distribution function
$F_{l,\mathrm{neg}}, F_{l,\mathrm{neu}}, F_{l,\mathrm{pos}}$ = fractions of particles which are charged negatively, neutral, or charged positively in lth discrete size regime or sectional size regime
$I(v)$ = nucleation rate of monomers
k_B = Boltzmann constant, 1.38×10^{-16}, gcm^2/s^{2}K
m_R = reduced mass between the moving particles
M = mass of species, g
$n(v,t)$ = size distribution function, cm^{-6}
N = number concentrations of species, cm^{-3}
N_l = number concentrations of particles in lth discrete size regime or sectional size regime, cm^{-3}
q_i = volume concentration variable for i-mers in the discrete size regime
Q_k = volume concentration variable for section k particles
S_1 = mass generation rate of monomers, g/cm^{3}s
t = time, s
T = temperature of species, K
T_g = gas temperature, 300 K
v = particle volume variable, cm^3
v_1 = monomer volume, cm^3
v_k = particle volume upper boundary of sectional k, cm^3
v_{k-1} = particle volume lower boundary of sectional k, cm^3
v_R = relative velocity between the moving particles
W = integral correction factor for coagulation between charged particles

$$= \frac{e^y - 1}{y},\ y = \frac{z_i z_j e^2}{\epsilon_0 k_B T_e (d_i + d_j)}$$ (Friedlander, 2000)

$x_{l,1} = (-0.5 - \bar{z}_l)/\sigma_l$
$x_{l,2} = (0.5 - \bar{z}_l)/\sigma_l$
z = particle charges, e
$\bar{z}_l$ = average charges of particle in lth discrete size regime or sectional size regime, e/particle

Greek letters

$\beta^*_{i,j}$ = general property coagulation coefficient [$\beta_{i,j}/(jv_1)$]
$\beta(u,v)$ = collision frequency function between particles (Friedlander, 2000)
$\bar{\beta}$ = collision integral for coagulations of two sectional size regime particles
$\bar{\beta}^D_{i,k}$ = collision integral for coagulations of section k particles and i-mers in discrete size regime
$\bar{\beta}^{DD}_{i,j,k}$ = collision integral for coagulations of two discrete size regime particles
ϵ_0 = permittivity of free space, 8.854×10^{-21}, C^2/dyn·cm^2
ρ_q = particle density, g/cm^3
σ_l^2 = variance in lth discrete size regime or sectional size regime
τ_{res} = residence time, s

Subscripts

0 = initial
e = electron
l = lth discrete size regime or sectional size regime
+ = positive ion
− = negative ion

Literature Cited

Adachi, M., K. Okuyama, and Y. Kousaka, "Electrostatic Coagulation of Bipolarly Charged Aerosol Particles," *J. Chem. Eng. Jpn.*, **14**, 467 (1981).

Bouchoule, A., and L. Boufendi, "High Concentration Effects in Dusty Plasma," *Plasma Sources Sci. Technol.*, **3**, 292 (1994).

Bouchoule, A., L. Boufendi, J. Hermann, A. Plain, T. Hbid, G. Kroesen, and W. W. Stoffels, "Formation of Dense Submicronic Clouds in Low Pressure Ar-SiH_4 RF Reactor: Diagnostics and Growth Processes from Monomers to Large Size Particulates," *Pure & Appl. Chem.*, **68**, 1121 (1996).

Boufendi, L., and A. Bouchoule, "Particle Nucleation and Growth in a Low-Pressure Argon-Silane Discharge," *Plasma Sources Sci. Technol.*, **3**, 262 (1994).

Childs, M. A., and A. Gallagher, "Small Particle Growth in Silane Radio-Frequency Discharge," *J. Appl. Phys.*, **87**, 1076 (2000).

Courteille, C., Ch. Hollenstein, J.-L. Dorier, P. Gay, W. Schwarzenbach, A. A. Howling, E. Bertran, G. Viera, R. Martins, and A. Macarico, "Particle Agglomeration Study in RF Silane Plasmas: *In Situ* Study by Polarization-Sensitive Laser Light Scattering," *J. Appl. Phys.*, **80**, 2069 (1996).

Friedlander, S. K., *Smoke, Dust and Haze*, Wiley-Interscience, New York (2000).

Fukuzawa, T., S. Kushima, Y. Matsuoka, M. Shiratani, and Y. Watanabe, "Growth of Particles in Cluster-Size Range in Low Pressure and Low Power SiH_4 RF Discharges," *J. Appl. Phys.*, **86**, 3543 (1999).

Gelbard, F., Y. Tambour, and J. H. Seinfeld, "Sectional Representations for Simulating Aerosol Dynamics," *J. Colloid Interface Sci.*, **76**, 541 (1980).

Girshick, S. L., "Theory on Nucleation from the Gas Phase by a Sequence of Reversible Chemical Reactions," *J. Chem. Phys.*, **107**, 1948 (1997).

Horanyi, M., and C. K. Goertz, "Coagulation of Dust Particles in a Plasma," *The Astrophysical J.*, **361**, 155 (1990).

Howling, A. A., L. Sansonnens, J.-L. Dorier, and Ch. Hollenstein, "Negative Hydrogenated Silicon Ion Clusters as Particle Precursors in RF Silane Plasma Deposition Experiments," *J. Phys. D: Appl. Phys.*, **26**, 1003 (1993).

Huang, F. Y., and M. J. Kushner, "Shapes of Agglomerates in Plasma Etching Reactors," *J. Appl. Phys.*, **81**, 5960 (1997).

Kasper, G., "Electrostatic Dispersion of Homopolar Charged Aerosols," *J. Colloid Interface Sci.*, **81**, 32 (1981).

Kim, D.-J., and K.-S. Kim, "Modeling of the Evolutions of Negative Ions in Silane Plasma Chemical Vapor Deposition for Various Process Conditions," *Jpn. J. Appl. Phys.*, **36**, 4989 (1997).

Kim, D.-J., and K.-S. Kim, "The Factors Affecting the Particle Distributions Inside the Silane PCVD Reactor for Semiconductor Processing," *Aerosol. Sci. Technol.*, **32**, 293 (2000a).

Kim, K.-S., and M. Ikegawa, "Particle Growth and Transport in Silane Plasma Chemical Vapor Deposition," *Plasma Sources Sci. Technol.*, **5**, 311 (1996).

Kim, K.-S., and D.-J. Kim, "Modeling of Rapid Particle Growth by Coagulation in Silane Plasma Reactor," *J. Appl. Phys.*, **87**, 1 (2000b).

Kobata, A., K. Kusakabe, and S. Morooka, "Growth and Transformation of TiO_2 Crystallites in Aerosol Reactor," *AIChE J.*, **37**, 347 (1991).

Kortshagen, U., and U. Bhandarkar, "Modeling of Particle Coagulation in Low Pressure Plasmas," *Phys. Rev. E.*, **60**, 887 (1999).

Landgrebe, J. D., and S. E. Pratsinis, "A Discrete-Sectional Model for Particle Production by Gas-Phase Chemical Reaction and Aerosol Coagulation in the Free-Molecular Regime," *J. Colloid Interface Sci.*, **139**, 63 (1990).

Lemons, D. S., R. K. Keinigs, D. Winske, and M. E. Jones, "Scaling Laws for Particle Growth in Plasma Reactors," *Appl. Phys. Lett.*, **68**, 613 (1996).

Lieberman, M. A., and A. J. Lichtenberg, *Principles of Plasma Discharges and Materials Processing*, Wiley-Interscience, New York (1994).

Matsoukas, T., and M. Russell, "Particle Charging in Low-Pressure Plasmas," *J. Appl. Phys.*, **77**, 4285 (1995).

Matsoukas, T., M. Russell, and M. Smith, "Stochastic Charge Fluctuations in Dusty Plasmas," *J. Vac. Sci. Technol.*, **A14**, 624 (1996).

Matsoukas, T., and M. Russell, "Fokker-Planck Description of Particle Charging in Ionized Gases," *Phys. Rev. E*, **55**, 991 (1997).

Riggs, J. B., *An Introduction to Numerical Methods for Chemical Engineers*, Texas Tech Univ. Press, TX (1988).
Samsonov, D., and J. Goree, "Particle Growth in a Sputtering Discharge," *J. Vac. Sci. Technol.*, **A17**, 2835 (1999).
Selwyn, G. S., "The Unconventional Nature of Particles," *Semicond. Int.*, **16**, 72 (1993).
Selwyn, G. S., "Optical Characterization of Particle Traps," *Plasma Sources Sci. Technol*, **3**, 340 (1994).
Shiratani, M., H. Kawasaki, T. Fukuzawa, H. Tsuruoka, T. Yoshioka, and Y. Watanabe, "Study on Growth Processes of Particulates in Helium-Diluted Silane RF Plasmas Using Electron Microscopy," *Appl. Phys. Lett.*, **65**, 1900 (1994).
Shiratani, M., T. Fukuzawa, and Y. Watanabe, "Formation Processes of Particulates in Helium-Diluted Silane RF Plasmas," *IEEE Trans. Plasma Sci.*, **22**, 103 (1994).
Shiratani, M., H. Kawasaki, T. Fukuzawa, H. Tsuruoka, T. Yoshioka, Y. Ueda, S. Singh, and Y. Watanabe, "Simultaneous In Situ Measurements of Properties of Particulates in RF Silane Plasmas Using a Polarization-Sensitive Laser-Light-Scattering Method," *J. Appl. Phys.*, **79**, 104 (1996).
Vemury, S., C. Jansen, and S. E. Pratsinis, "Coagulation of Symmetric and Asymmetric Bipolar Aerosols," *J. Aerosol Sci.*, **28**, 599 (1997).
Watanabe, Y., "Dust Phenomena in Processing Plasmas," *Plasma Phys. Control. Fusion*, **39**, A59 (1997).
Watanabe, Y., M. Shiratani, T. Fukuzawa, H. Kawasaki, Y. Ueda, S. Singh, and H. Ohkura, "Contribution of Short Lifetime Radicals to the Growth of Particles in SiH_4 High Frequency Discharges and the Effects of Particles on Deposited Films," *J. Vac. Sci. Technol.*, **A14**, 995 (1996).
Watanabe, Y., M. Shiratani, H. Kawasaki, S. Singh, T. Fukuzawa, Y. Ueda, and H. Ohkura, "Growth Processes of Particles in High Frequency Silane Plasmas," *J. Vac. Sci. Technol.*, **A14**, 540 (1996).
Wu, C.-Y., and P. Biswas, "Study of Numerical Diffusion in a Discrete-Sectional Model and Its Application to Aerosol Dynamics Simulation," *Aerosol. Sci. Technol.*, **29**, 359 (1998).
Wu, J. J., and R. C. Flagan, "A Discrete-Sectional Solution to the Aerosol Dynamic Equation," *J. Colloid Interface Sci.*, **123**, 339 (1988).
Xiong, Y., S. E. Pratsinis, and S. V. R. Mastrangelo, "The Effect of Ionic Additives on Aerosol Coagulation," *J. Colloid Interface Sci.*, **153**, 106 (1992).

Manuscript received Oct. 1, 2001, and revision received Apr. 16, 2002.